

---

# Search for WHIM around A2744 using Suzaku

Shiho HATTORI<sup>1</sup>, Naomi OTA<sup>1</sup>, Yu-Ying ZHANG<sup>2</sup>, Hiroki AKAMATSU<sup>3</sup> and Alexis FINOGENOV<sup>4,5</sup>

<sup>1</sup>Department of Physics, Nara Women’s University, Kita-uoyanishi-machi, Nara, Nara 630-8506, Japan

<sup>2</sup>Argelander Institute for Astronomy, Bonn University, Auf dem Hügel 71, 53121 Bonn, Germany

<sup>3</sup>SRON Netherlands Institute for Space Research, Sorbonnelaan 2, 3584 CA Utrecht, The Netherlands

<sup>4</sup>Max-Planck-Institut für extraterrestrische Physik, Giessenbachstraße, 85748 Garching, Germany

<sup>5</sup>Department of Physics, University of Helsinki, Gustaf Hällströmin katu 2a, FI-00014 Helsinki, Finland

Received ; Accepted

## Abstract

We present the results from the Suzaku satellite of the surrounding region of a galaxy cluster, A2744, at  $z = 0.3$ . To search for oxygen emission lines from the warm-hot intergalactic medium (WHIM), we analyzed X-ray spectra from two northeast regions 2.2–3.3 and 3.3–4.4 Mpc from the center of the cluster, which offers the first test on the presence of a WHIM near the typical accretion shock radius ( $\sim 2r_{200}$ ) predicted by hydrodynamical simulations. For the 2.2–3.3 Mpc region, the spectral fit significantly (99.2% significance) improved when we include O VII and O VIII lines in the spectral model. A comparable WHIM surface brightness was obtained in the 3.3–4.4 Mpc region and the redshift of O VIII line is consistent with  $z = 0.3$  within errors. The present results support that the observed soft X-ray emission originated from the WHIM. However, considering both statistical and systematic uncertainties, O VIII detection in the northeast regions was marginal. The surface brightness of the O VIII line in  $10^{-7}$  photons  $\text{cm}^{-2}\text{s}^{-1}\text{arcmin}^{-2}$  was measured to be  $2.7 \pm 1.0$ ,  $2.1 \pm 1.2$  for the 2.2–3.3, 3.3–4.4 Mpc regions, giving the upper limit on the baryon overdensity of  $\delta = 319 (< 443)$ ,  $283 (< 446)$ , respectively. This is comparable with previous observations of cluster outskirts and their theoretical predictions. The future prospect for WHIM detection using the Athena X-IFU microcalorimeter is briefly discussed here. In addition, we also derived the ICM temperature distribution of A2744 to detect a clear discontinuity at the location of the radio relic. This suggests that the cluster has undergone strong shock heating by mass accretion along the filament.

**Key words:** cosmology: observations — large-scale structure of universe — intergalactic medium — galaxies: clusters: individual (Abell 2744) — X-rays: galaxies: clusters

---

## 1 Introduction

In the present Universe, the baryon mass falls short of the most likely value predicted by Big Bang nucleosynthesis by a factor of 2; this is called the “missing baryon problem” (Fukugita

et al. 1998). Numerical simulations predict that a large fraction of baryons should be in the form of warm-hot intergalactic medium (WHIM) with temperature  $10^5 - 10^7$  K and have a very diffuse distribution (Cen & Ostriker 1999). The baryon

overdensity, a ratio between the hydrogen density and its mean value in the Universe,  $\delta \equiv n_{\text{H}}/\bar{n}_{\text{H}}$ , is predicted to be 10 – 500 for the WHIM (Cen & Ostriker 1999; Shull et al. 2012). The detection of this missing warm-hot gas is not only a key to resolving the discrepancy of the total amount of baryons between the nearby and distant universe but also to understand their evolution.

Identification of the WHIM is a challenge given its very low surface brightness and the current sensitivities of the available instruments (see Bregman 2007 for a review). At  $10^5 - 10^7$  K, emission or absorption lines from ionized atoms may be detectable in the soft X-ray and ultraviolet regimes. In particular, oxygen is the most abundant heavy element, X-ray spectroscopy of O VII and O VIII lines can then provide an important clue in the search for the WHIM. Since the WHIM is expected to be most dense around clusters of galaxies, the analysis of soft X-ray emission in and near such objects has been carried out.

Possible detections of redshifted O VII line emission in 7 clusters of galaxies have been reported by Kaastra et al. (2003); Kaastra (2004) based on XMM-Newton observations. Takei et al. (2007) observed the surrounding regions of A2218 at  $z = 0.18$  using Suzaku and derived an upper limit of the O VII and O VIII fluxes that is significantly lower than previous measurements, yielding an overdensity of  $\delta < 270$ . Using XMM-Newton, Werner et al. (2008) detected X-ray emission from the filament connecting the double cluster A222/A223, which corresponds to  $\delta \sim 150$ , while Mitsuishi et al. (2012) found no significant WHIM emission in a region between A3558 and A3556, giving an upper limit of  $\delta < 380$ . Recently, based on long XMM-Newton observations, Eckert et al. (2015) discovered hot gas that coincides with the overdensities of galaxies and dark matter in the filaments around A2744, suggesting that a large fraction of the cosmic baryons are located in the cosmic web.

A2744 (AC118 or RXC J0014.3–3022; Böhringer et al. 2004) is an active merging galaxy cluster at  $z = 0.308$  with a complex mass structure and is also known as “Pandora’s cluster” (e.g., Owers et al. 2011). The precise lensing mass distribution has been determined by utilizing the deepest HST data from the Frontier Fields program (Jauzac et al. 2015; Wang et al. 2015). Large-scale galaxy filaments in the south and northwest directions were first noted by Braglia et al. (2007). Spectroscopically identified 343 member galaxies within 3 Mpc from the cluster center were catalogued by Owers et al. (2011), with which a galaxy concentration in the east-northeast was also recognized. Using Suzaku, Ibaraki et al. (2014) measured the intracluster medium (ICM) temperature distribution in the three directions out to a virial radius of  $r_{200} = 2$  Mpc and found that there was not a clear temperature decrease in the cluster’s outskirts, unlike many other clusters (Reiprich et al. 2013). They also pointed out the presence of high-temperature gas in the

northeast region whose location coincides with a large radio relic (Orrú et al. 2007), suggesting that the cluster has experienced shock heating due to a merger or mass accretion.

In this paper, we will analyze X-ray spectra taken from deep Suzaku observations of the A2744 northeast region with the aim of studying the WHIM emission as well as the thermodynamical properties of the ICM. Since this follow-up observation covered a wider area in comparison with the previous X-ray observations, we can not only examine the WHIM emission reported by XMM-Newton, but can also extend the measurements out to 4.4 Mpc from the cluster’s center. This will provide the first test on the presence of warm-hot gas near  $r = 2r_{200}$ , which corresponds to the typical radius where accretion shock occurs (Lau et al. 2015). The X-ray Imaging Spectrometer (XIS; Koyama et al. 2007) onboard Suzaku (Mitsuda et al. 2007) has the lowest background level available. In addition to the improved energy resolution in the soft X-ray band, it is suited for studying faint diffuse emission from warm/hot gas beyond the cluster virial radius. To complement the spatial resolution of Suzaku’s X-ray telescopes, XMM-Newton data were utilized to eliminate contamination from point sources in the field.

Throughout this paper, we will adopt the following cosmological parameters,  $H_0 = 70 \text{ km s}^{-1} \text{ Mpc}^{-1}$ ,  $\Omega_M = 0.27$ , and  $\Omega_\Lambda = 0.73$ .  $1' = 274 \text{ kpc}$  at a cluster redshift of  $z = 0.308$  (The NASA/IPAC Extragalactic Database). The quoted errors are at the  $1\sigma$  confidence level unless otherwise stated. The solar abundance table by Anders & Grevesse (1989) was assumed.

## 2 Observation and data reduction

We conducted a follow-up observation of the A2744 northeast filament using Suzaku for 83 ksec and performed data analysis in combination with the previous central and southern pointing observations. Table 1 provides the observation log. The data taken using two front-side illuminated CCDs (XIS-0, XIS-3) and one backside illuminated CCD (XIS-1) were reduced in the standard manner by using HEASoFT version 6.17 and a calibration database released on 2015 October 5.

Since we are interested in soft X-ray emission from the intergalactic medium, we have to pay attention to possible contamination from neutral oxygen lines produced in the Earth’s atmosphere (Sekiya et al. 2014; Yoshitake et al. 2013). The spectral analysis was performed with changing the data screening criteria of the minimum elevation angle from the limb of the day Earth, DYE\_ELV, from  $20^\circ$  to  $50^\circ$ . The O I line flux significantly reduced if the threshold was changed from  $20^\circ$  to  $30^\circ$ , and statistically consistent fitting results were obtained if  $\text{DYE\_ELV} > 30^\circ$ . Thus we show results based on the data selection with  $\text{DYE\_ELV} > 30^\circ$  in the present paper. Systematic uncertainties in the WHIM measurement are examined in §3.2 in more detail.

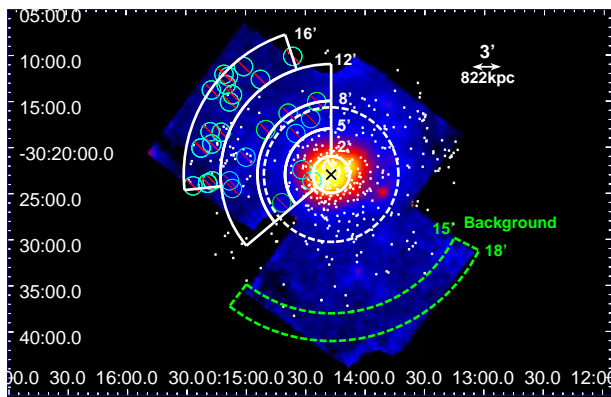


**Fig. 1.** Suzaku XIS-0 + XIS-1 + XIS-3 mosaic image of A2744 in the 0.5–10 keV band. The background is not subtracted but the image is corrected for the exposure map and vignetting effects. The X-ray centroid of the cluster emission is marked by “x”. The white sectors are the spectral integration regions for ICM and WHIM analyses, while the green sector was used to model background spectra. The cyan circles denote point sources detected by XMM-Newton, which were excluded with an  $r = 1'$  radius from the spectral integration regions. The virial radius is indicated by the dashed white circle. The positions of member galaxies with redshifts within  $cz \pm 5000 \text{ km s}^{-1}$  ( $z = 0.308$ ) and the  $r_F$ -band magnitude  $r_F < 23$  (Owers et al. 2011) are marked by the white dots.

The CCD flickering pixels were removed according to a recipe provided by the XIS instrument team<sup>1</sup>. During the Suzaku observations of A2744 Northeast, XIS light curves were stable and the solar-wind proton flux measured by the ACE satellite,  $< 2 \times 10^8 \text{ cm}^{-2} \text{ s}^{-1}$ , agree with that of the quiescent phase (Fujimoto et al. 2007). Thus the present data is unlikely to be affected by the solar activity.

The XIS mosaic image in the 0.5–10 keV band is shown in Figure 1. As the virial radius is estimated as  $r_{200} = 2.0 \text{ Mpc}$  or  $7'.3$  (Ibaraki et al. 2014), the northeast pointing covers a large radial range that is  $0 - 2.2r_{200}$  from the cluster’s center. To search for diffuse WHIM emission beyond the cluster’s virial radius, two sectors at  $8' - 12'$  and  $12' - 16'$  were defined as filament regions because the northeastern galaxy concentration at around  $r \sim 10'$  was noted by the galaxy density map (Owers et al. 2011; Ibaraki et al. 2014). To measure the ICM temperature profile across the radio relic at  $r = 7'$ , additional three integration regions,  $0' - 2'$ ,  $2' - 5'$ ,  $5' - 8'$  were defined as indicated in the figure.

The XIS spectra in each region were extracted from the cleaned XIS event files. Since the three regions at  $0' - 2'$ ,  $2' - 5'$ ,  $5' - 8'$  were covered by both Center and Northeast observations, the spectra extracted from these two data sets were co-added. The spectra were rebinned so that each spectral bin contained more than 20 source counts. The X-ray telescope and CCD responses were calculated using `xissimarfgen` and `xisrmfgen`, respectively. Non-X-ray background produced by `xisnxbgen` was subtracted from the spectra. Point sources in the XIS fields

<sup>1</sup> [http://www.astro.isas.jaxa.jp/suzaku/analysis/xis/nxb\\_new2/](http://www.astro.isas.jaxa.jp/suzaku/analysis/xis/nxb_new2/)

were searched by utilizing the XMM-Newton PN and MOS data (OBSID 0743850101), and detected sources whose fluxes are larger than  $2 \times 10^{-14} \text{ erg s}^{-1} \text{ cm}^{-2}$  were removed from the XIS data with an  $r = 1'$  circle. In the case that the extraction radius was changed from  $1'$  to  $1'.5$ , we confirmed that the present results were not significantly affected.

We derived the background model by fitting the spectra in the southern region ( $15' < r < 18'$ ) to the same model as used by Ibaraki et al. (2014). The model function is composed of the cosmic X-ray background (CXB) and the galactic X-ray background (GXB) from the Milky Way halo (MWH) and the Local Hot Bubble (LHB) and is represented by “`apecLHB+phabs(apecMWH+power-lawCXB)`”. Here, the MWH and LHB temperatures were fixed at 0.34 and 0.13 keV, respectively, and the power-law index of the CXB component was fixed at 1.4. The hydrogen column density of the galactic absorption was fixed at  $N_{\text{H}} = 1.39 \times 10^{20} \text{ cm}^{-2}$  (Kalberla et al. 2005). The fitting result is shown in Figure 2. The model parameters are listed in Table 2, which agree with those obtained from previous Suzaku analysis (Ibaraki et al. 2014) and XMM-Newton observations within their errors (Eckert et al. 2015).

We also analyzed two offset XIS fields located at about  $3^\circ$  away from the A2744 center (OBSID: 506028010, 506029010) to find their CXB and GXB models are consistent with those presented in Table 2 and their best-fit parameters agree within 10%. Therefore we decided to take  $\pm 10\%$  as the systematic error on the background model.

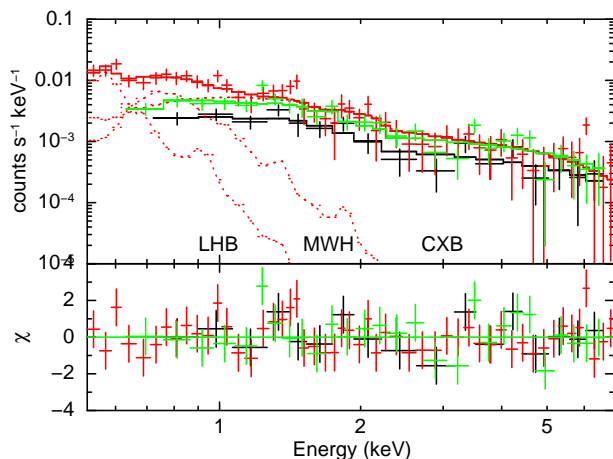


**Fig. 2.** XIS background spectra with subtracted non-X-ray background component. XIS-0, XIS-1 and XIS-3 are shown using black, red, and green crosses, respectively. The solid and dashed lines represent the total model and the background components for XIS-1, respectively.

### 3 Search for WHIM emission

#### 3.1 Analysis of WHIM emission spectra

To search for WHIM emission in the northeast of A2744, we analyzed the XIS spectra from the  $r = 8' - 12'$  ( $= 1.1r_{200} -$

**Table 1.** Log of Suzaku observations

Object	OBSID	Date	(RA, Dec)	Exposure (s) <sup>a</sup>
A2744 Center	802033010	2007 May 19–23	(00:14:9.5, -30:20:40.6)	153 241
A2744 South	805015010	2010 Dec. 10–12	(00:14:3.2, -30:33:2.9)	69 776
A2744 Northeast	808008010	2013 Nov. 20–22	(00:14:52.5, -30:18:28.1)	82 781

<sup>a</sup> Exposure time after data filtering.

**Table 2.** Background model parameters

$\Gamma$	$Norm^a$ ( $\times 10^{-4}$ )	$kT_{MWH}$ [keV]	$Norm^b$ ( $\times 10^{-4}$ )	$kT_{LHB}$ [keV]	$Norm^b$ ( $\times 10^{-3}$ )	$\chi^2/d.o.f.$
1.4(fixed)	$6.58^{+0.54}_{-0.54}$	0.34(fixed)	$3.35^{+0.60}_{-0.56}$	0.13(fixed)	$1.71^{+0.35}_{-0.32}$	77.5/92

<sup>a</sup>Normalization of power-law model [photons  $\text{keV}^{-1} \text{cm}^{-2} \text{s}^{-1}$ ]. <sup>b</sup>Normalization of APEC model,  $Norm = \int n_e n_H dV / (4\pi(1+z)^2 D_A^2)$  [ $10^{-14} \text{cm}^{-5}$ ].  $D_A$  is the angular diameter distance to the source. An  $r = 20'$  uniform sky is assumed.

$1.6r_{200}$ ) and  $r = 12' - 16'$  ( $= 1.6r_{200} - 2.2r_{200}$ ) regions (Figure 1). This enabled us to examine the presence of WHIM near  $r = 2r_{200}$ , corresponding to the typical location of the accretion shock as suggested by hydrodynamical simulations (Lau et al. 2015). In this analysis, only XIS-1 data were used because it has a higher sensitivity in the soft X-ray band than other XIS sensors.

First, the WHIM emission in the filament spectrum was modeled in two ways: i) the APEC thin-thermal plasma model (Smith et al. 2001) and ii) two Gaussian functions for the redshifted O VII and O VIII lines. In case i), the metal abundance was fixed at  $Z = 0.2$  solar because the median oxygen metallicity is 0.18 solar (Cen & Ostriker 2006). In the outermost region ( $12' < r < 16'$ ), the temperature was not well constrained and fixed at the typical value of  $kT_1 = 0.2$  keV since the O VIII line is the strongest at this temperature. In case ii), the line centroid energies were fixed at 0.439 keV and 0.500 keV and the line width was fixed at  $\sigma = 0$ . Since the WHIM emission is faint, we fitted the filament and background spectra in the 0.4–7 keV band simultaneously assuming that the background model is common between the two regions instead of subtracting it directly from the filament data. Except for the three normalization factors, the background model parameters were fixed at the values shown in Table 2. The  $\chi^2$  fitting was performed using XSPEC version 12.9.0<sup>2</sup>. The XIS spectra are shown in Figure 3, and model parameters for i) the APEC model and ii) the Gaussian model are shown in Table 3.

In comparison with the fit using the background-only model ( $\chi^2/d.o.f. = 130.0/95$  and  $93.8/79$  for  $r = 8' - 12'$  and  $12' - 16'$ , respectively), we examined the improvement of the spectral fit by adding the WHIM model using the F-test (Table 4). The F-statistic values were i) 15.7 and ii) 6.6 for 2 additional model parameters. Thus the WHIM component is statistically significant at the  $> 99.99\%$  and  $99.8\%$  levels.

We should note that the gas temperature at  $r = 8' - 12'$  de-

rived under i) the APEC model,  $kT_1 = 1.7^{+0.35}_{-0.15}$  keV, is higher than that predicted for the WHIM (Cen & Ostriker 1999) and positive residuals are seen at around 0.5 keV, while ii) the Gaussian model left positive residuals in consecutive data points at 1–2 keV. Thus, in order to test a possibility that the observed spectrum is represented by a superposition of ICM and WHIM emissions, we fit the XIS-1 spectra by assuming iii) a two-component model consisting of an APEC model for the ICM and two Gaussian lines for the WHIM. The result is shown in Table 3 and Figure 4. In comparison with the case i), the improvement of the spectral fit by adding the WHIM component is significant at 99.2% by F-test. We also confirmed that a reasonable fit is obtained if the Gaussian lines were replaced by a  $Z = 0.2$  solar APEC model, resulting the best-fit WHIM temperature of  $kT_2 = 0.27^{+0.09}_{-0.05}$  keV and  $\chi^2/d.o.f. = 95.6/91$  (model iv in Table 3). Therefore we suggest that the observed soft X-ray spectra can be well reproduced by a sum of  $kT_1 \sim 1.7$  keV ICM and  $kT_2 \sim 0.2 - 0.4$  keV WHIM.

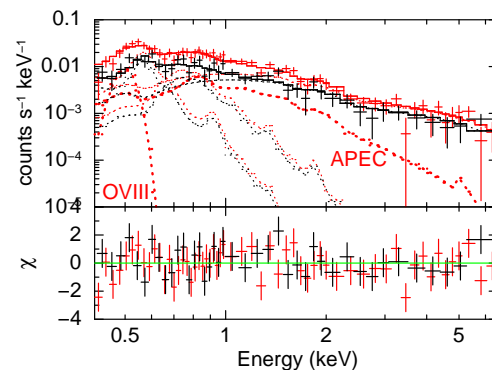


**Fig. 4.** XIS-1 spectrum of the A2744 north-east filament  $8' < r < 12'$  (red) and the background region (black). The total model (the solid line) is composed of GXB+CXB (thin dotted lines) and iii) the APEC model and Gaussian lines (thick dotted lines).

For  $r = 12' - 16'$ , i) and ii) provided a reasonably good fit to the data. In comparison with the fit using the background-only model, the F-values were i) 1.1 for one additional parameter and

<sup>2</sup> XSPEC version 12.9.0a was used when we analyzed the WHIM component under the APEC model with  $z \neq 0$ .

**Table 3.** Model parameters for the A2744 northeast filament

Model	$r$ [arcmin]	APEC <sup>a</sup>		APEC <sup>a</sup>		Gaussian, O VIII <sup>b</sup>	Gaussian, O VII <sup>b</sup>	$\chi^2/\text{d.o.f.}$
		$kT_1$ [keV]	$Norm_1$ ( $\times 10^{-3}$ )	$kT_2$ [keV]	$Norm_2$ ( $\times 10^{-3}$ )	$Norm^c$ ( $\times 10^{-4}$ )	$Norm^c$ ( $\times 10^{-4}$ )	
i)	8–12	$1.73^{+0.35}_{-0.15}$	$2.85^{+0.49}_{-0.50}$	–	–	–	–	97.3/93
i)	12–16	0.2 (fixed)	$1.51^{+1.32}_{-1.32}$	–	–	–	–	92.5/78
ii)	8–12	–	–	–	–	$4.22^{+1.05}_{-1.05}$	< 0.39	113.9/93
ii)	12–16	–	–	–	–	$2.65^{+1.28}_{-1.28}$	< 1.65	89.5/77
iii)	8–12	$1.73^{+0.50}_{-0.16}$	$2.60^{+0.48}_{-0.51}$	–	–	$3.35^{+1.04}_{-1.10}$	< 0.32	87.5/91
iv)	8–12	$1.74^{+0.47}_{-0.15}$	$2.55^{+0.55}_{-0.51}$	$0.27^{+0.09}_{-0.05}$	$1.45^{+1.01}_{-1.01}$	–	–	95.6/91

<sup>a</sup>The metal abundance was fixed at 0.2 solar. <sup>b</sup>Centroid energies of the redshifted emission lines were assumed to be 0.500 keV and 0.439 keV for the O VIII and O VII lines, respectively. Their rest-frame energies are 0.654 and 0.574 keV. <sup>c</sup>Gaussian line flux [ $\text{photons cm}^{-2}\text{s}^{-1}$ ].

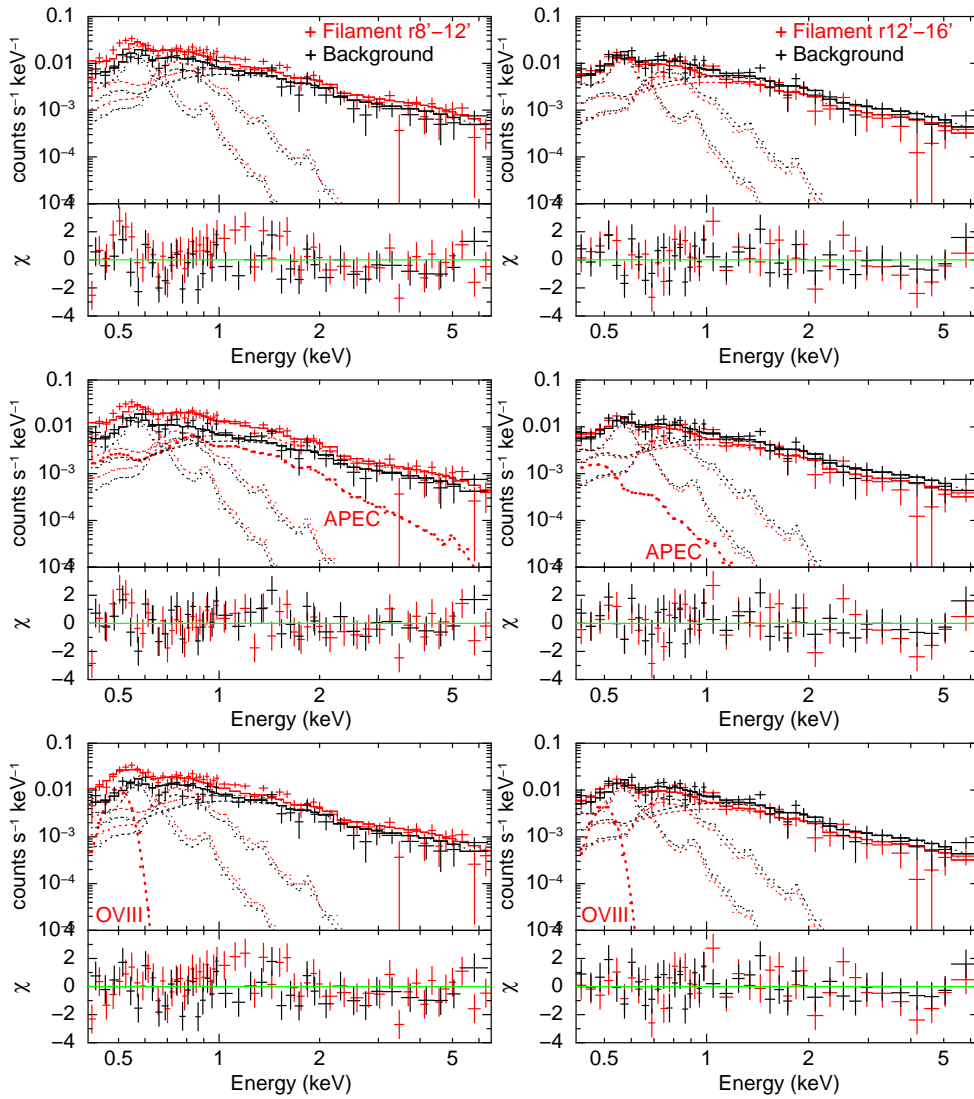


**Fig. 3.** Left: XIS-1 spectra of the A2744 north-east filament  $8' < r < 12'$  (red) and the background region (black). Right: XIS-1 spectra of the A2744 north-east filament  $12' < r < 16'$  (red) and the background region (black). In the upper panels, the total model (the solid line) is composed of GXB and CXB (thin dotted lines). In the middle panels, the total model incorporates i) the additional APEC model for the WHIM (thick dotted line). In the bottom panels, the total model incorporates ii) the additional two Gaussian lines for the WHIM (thick dotted line).

**Table 4.** Surface brightness of the WHIM and the statistical significance by F-test

$r$ [arcmin]	Model component	$I^a$	$I(2\sigma \text{ limit})^b$	$F^c$	Probability <sup>c</sup>	$\delta^d$	$\delta(2\sigma \text{ limit})^e$
8–12	i) APEC	$6.67 \pm 1.14 \pm 1.94$	$< 11.2$	15.7	$1.4 \times 10^{-6}$	$199 \pm 17 \pm 26$	$< 261$
8–12	ii) Gaussian, O VIII	$3.36 \pm 0.84 \pm 0.70$	$< 5.5$	6.60	0.002	$358 \pm 44 \pm 38$	$< 474$
	Gaussian, O VII	$0.00 \pm 0.31 \pm 0.00$	$< 0.6$			$0 \pm 93 \pm 0$	$< 132$
8–12	iii) Gaussian, O VIII	$2.67 \pm 0.85 \pm 0.60$	$< 4.8$	5.08	0.008	$319 \pm 50 \pm 36$	$< 443$
	Gaussian, O VII	$0.00 \pm 0.25 \pm 0.00$	$< 0.5$			$0 \pm 85 \pm 0$	$< 120$
8–12	iv) APEC	$2.57 \pm 1.79 \pm 2.15$	$< 8.2$	0.81	0.45	$166 \pm 58 \pm 70$	$< 348$
12–16	i) APEC ( $kT_1$ fix)	$2.08 \pm 1.82 \pm 1.67$	$< 7.0$	1.10	0.30	$145 \pm 63 \pm 60$	$< 319$
12–16	ii) Gaussian, O VIII	$2.11 \pm 1.02 \pm 0.65$	$< 4.5$	1.86	0.16	$283 \pm 68 \pm 44$	$< 446$
	Gaussian, O VII	$0.00 \pm 1.31 \pm 0.00$	$< 2.6$			$0 \pm 193 \pm 0$	$< 272$

<sup>a</sup>The surface brightness of the WHIM component in units of  $10^{-7}$  photons  $\text{cm}^{-2} \text{s}^{-1} \text{arcmin}^{-2}$ . The first and second errors are the  $1\sigma$  statistical and systematic uncertainties. The brightness was calculated in the 0.4–7 keV band for the APEC model. <sup>b</sup>The  $2\sigma$  upper limit on the surface brightness of the WHIM component. Both statistical and systematic errors were taken into account. <sup>c</sup>The F-statistic value and the probability of finding a higher F-value than observed (see text). <sup>d</sup>The baryon overdensity and the  $1\sigma$  statistical and systematic uncertainties. <sup>e</sup>The  $2\sigma$  upper limit on the baryon overdensity.

ii) 1.9 for two additional parameters and the improvement was not significant at the 95% level.

If the redshift of oxygen lines was allowed to vary, the spectral fit gave the centroid energy of the redshifted O VIII line  $E_0 = 0.522 \pm 0.009 \pm 0.005$ ,  $0.514 \pm 0.017 \pm 0.005$  keV or  $z = 0.253 \pm 0.023 \pm 0.012$ ,  $0.272 \pm 0.044 \pm 0.012$  for  $r = 8' - 12'$ ,  $12' - 16'$ . Here the first and second errors represent the  $1\sigma$  statistical and systematic uncertainties. The latter was estimated by fitting the O I line spectra taken at  $10^\circ < \text{DYE\_ELV} < 20^\circ$  to the Gaussian line. Since the observed O I line energy is found to be systematically higher by 5 eV, we assign the  $1\sigma$  systematic error of 5 eV to the line energy<sup>3</sup>. Therefore the fitted redshifts are marginally lower than the cluster redshift  $z = 0.308$  but agree with the mean optical redshift of the northeast filament region,  $z = 0.3$ , (Owers et al. 2011) within  $1.8\sigma$ ,  $0.6\sigma$  for the two regions, respectively. This further supports that the soft X-ray emission in the filament region originates from the WHIM at  $z = 0.3$ .

Note that we repeated the analysis by fitting unbinned XIS spectra with the C-statistics and confirmed that the above results on the surface brightness and the centroid energy of the O VIII line were not affected by the choice of fitting methods.

### 3.2 WHIM surface brightness and systematic uncertainties

The surface brightness of the WHIM emission,  $I$ , derived from the spectral analysis is listed in Table 4, where the first and second errors refer to the  $1\sigma$  statistical and systematic uncertainties. The latter was estimated in the following manner.

We first consider two possible sources of systematic errors: a) uncertainty in the background modeling and b) degradation of XIS's low-energy efficiency due to contaminating material on the optical blocking filter. We then examine c) possible con-

tamination from the neutral oxygen lines.

For a), since the GXB also has strong oxygen lines, we intentionally changed the GXB intensity by  $\pm 10\%$  (see §2). For b), by comparing a measured thickness of the contaminant with a model used in the response generation (The Suzaku Technical Description Sec 7), the uncertainties in absorption column densities of carbon, nitrogen, and oxygen are estimated to be  $\pm 10\%$ . To take this into account, the absorption column densities were included in the spectral model. The total systematic error in the surface brightness was then calculated by adding the above two errors in quadrature.

As a result, for  $r = 8' - 12'$ , the WHIM brightness in photons  $\text{cm}^{-2} \text{s}^{-1} \text{arcmin}^{-2}$  was obtained as ii)  $I = (3.36 \pm 0.84 \pm 0.70) \times 10^{-7}$  and iii)  $I = (2.67 \pm 0.85 \pm 0.60) \times 10^{-7}$  for the O VIII line model. Thus, the O VIII emission is statistically significant at the  $3.1 - 4.0\sigma$  level. For  $r = 12' - 16'$ , though the WHIM brightness derived under the two models, i)  $I = (2.08 \pm 1.82 \pm 1.67) \times 10^{-7}$  and ii)  $I = (2.11 \pm 1.02 \pm 0.65) \times 10^{-7}$ , is comparable to that in the  $r = 8' - 12'$  region, the statistical significance of the O VIII line was lower ( $2.1\sigma$ ). Hence the detection of the WHIM component is marginal if systematic uncertainty is considered.

For c), as mentioned in §2, the fitting results for the WHIM component were not affected by the data screening criteria if  $\text{DYE\_ELV} > 30^\circ$  was applied. This suggests that the present data is less contaminated by the O I line emission. Given the current instrumental resolution and photon statistics, however, the line centroid energy derived from the Gaussian fitting indicates that the O I line at 0.525 keV cannot be completely distinguished from the redshifted O VIII line at 0.500 keV. For example, if the O VIII line was replaced with the O I line at 0.525 keV, we obtained an acceptable fit to the  $r = 12' - 16'$  spectra ( $\chi^2/\text{d.o.f.} = 89/78$ ).

To check how much the WHIM surface brightness is affected by the possible O I contamination, we added another Gaussian line at 0.525 keV to iii) the APEC and Gaussian models for  $r =$

<sup>3</sup> The typical calibration error of the XIS energy scale in the soft X-ray band is 5 eV (<http://www.astro.isas.jaxa.jp/suzaku/process/caveats/>)

**Table 5.** APEC model parameters for the ICM in the northeast.

$r$ [arcmin]	$kT$ [keV]	Abundance [solar]	Norm ( $\times 10^{-3}$ )	$\chi^2/\text{d.o.f.}$
0–2	$9.79^{+0.15}_{-0.15}$	$0.23^{+0.02}_{-0.02}$	$6.63^{+0.04}_{-0.04}$	2036.7/2141
2–5	$8.84^{+0.37}_{-0.36}$	$0.21^{+0.04}_{-0.04}$	$5.71^{+0.08}_{-0.08}$	683.3/681
5–8	$9.01^{+1.66}_{-1.24}$	$0.04^{+0.17}_{-0.04}$	$1.12^{+0.06}_{-0.07}$	229.6/241
8–12	$1.72^{+0.24}_{-0.11}$	0.2(fixed)	$0.49^{+0.09}_{-0.09}$	161.2/167

$8' - 12'$  and ii) the Gaussian model for  $12' - 16'$  (§3.1) and fitted the XIS spectra again. This yielded a lower O VIII brightness with a large statistical error:  $I = (0.12 \pm 0.76 \pm 0.07) \times 10^{-7}$ ,  $(0.93 \pm 1.37 \pm 0.77) \times 10^{-7}$  photons  $\text{cm}^{-2} \text{s}^{-1} \text{arcmin}^{-2}$  for the above regions, respectively.

## 4 Analysis of ICM temperature profile

The previous Suzaku analysis suggested the existence of very hot, shock-heated gas with  $kT = 13.6^{+9.6}_{-6.7}$  keV (90% error including the systematic uncertainty due to point source subtraction) that coincided with the location of the large radio relic. To improve the measurement accuracy and examine the shock structure, we derived a radial profile of the ICM temperature out to  $r = 12'$  in the northeast direction based on a follow-up observation. Note that the outermost sector at  $r = 8' - 12'$  is common to one of the filament regions defined in §2 and analyzed in §3.

The observed 0.7–7 keV spectra of three sensors (XIS-0, XIS-1, and XIS-3) were fitted using the APEC model corrected for the Galactic absorption. The background in each annular region was simulated by assuming the best-fit CXB+GXB parameters (Table 2) and were subtracted from the XIS spectra (§4). The redshift and Galactic hydrogen column density were fixed at  $z = 0.308$  and  $N_{\text{H}} = 1.39 \times 10^{20} \text{ cm}^{-2}$  (Kalberla et al. 2005). The ICM temperature, metal abundance, and the normalization factor were treated as free parameters. The best-fit model parameters are given in Table 5 and the temperature profile is plotted in Figure 5. The temperature ranged between 8–10 keV inside the virial radius. The temperature of  $9.0^{+1.7}_{-1.2}$  keV at  $5' < r < 8'$  is statistically consistent with previous results (Ibaraki et al. 2014) and that of the relic region,  $12.3^{+4.5}_{-3.5}$  keV, reported based on the joint Suzaku and XMM-Newton analysis (Eckert et al. 2016). On the other hand, the temperature is a factor of  $5.2 \pm 1.0$  lower outside that radius, i.e.,  $1.72^{+0.24}_{-0.11}$  keV. This ICM temperature agrees well with that obtained from the XIS spectral analysis under the model i) or iii) in §3.1 and is comparable to that reported from the XMM-Newton measurement of hot gas at the eastern galaxy concentration,  $T = (15 \pm 2) \times 10^6 \text{ K}$  (Eckert et al. 2015). Our Suzaku observation confirms the presence of a clear temperature drop across the relic. The nature of this structure is discussed in §5.3.

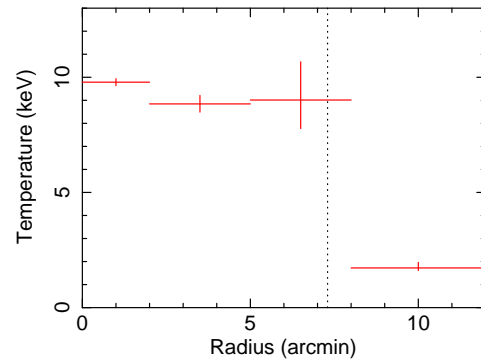


**Fig. 5.** ICM temperature profile in the A2744 northeast region as a function of distance from the cluster center (arcmin). The dashed line indicates the virial radius.

## 5 Discussion

We analyzed the X-ray spectra obtained from Suzaku's follow-up observation of the A2744 northeast filament regions and found that the soft X-ray spectrum at  $r = (1.1 - 1.6)r_{200}$  is significantly better fitted by adding the WHIM emission model, although the background uncertainty is not negligible. We also measured the WHIM emission near the typical accretion radius ( $2r_{200}$ ) for the first time. The redshift of O VIII line is consistent with  $z = 0.3$  within errors, suggesting that the observed soft X-ray emission originated from the WHIM. The detection was, however, not significant under the present measurement errors. Thus, we will derive the upper limit of the baryon overdensity in §5.1 and will discuss the prospect of the search for WHIM using the future X-ray mission in §5.2. The ICM temperature profile exhibits a clear drop at the location of radio relic. We will estimate the Mach number of the shock and compare it with radio observations in §5.3.

### 5.1 Estimation of the WHIM density

The baryon overdensity  $\delta = n_{\text{H}}/\bar{n}_{\text{H}}$  at a large distance from the A2744 center can be calculated by utilizing the same equations as used in the study of A2218 (Takei et al. 2007):

$$I = C(T)(1+z)^{-3}n_e n_{\text{H}} Z L, \quad (1)$$

$$\bar{n}_{\text{H}} = 1.77 \times 10^{-7} (1+z)^3 \text{ cm}^{-3}, \quad (2)$$

where  $I$  is the surface brightness of the warm-hot gas,  $C(T)$  is the line emissivity which depends on the warm-hot gas temperature  $T$  and calculated by the AtomDB database 3.0.2<sup>4</sup>,  $n_e$  is the electron density,  $n_{\text{H}}$  is the hydrogen density ( $n_e/n_{\text{H}} = 1.2$ ),  $Z$  is the metal abundance assuming the solar abundance table by Anders & Grevesse (1989)<sup>5</sup>, and  $L$  is the path length. We adopt  $kT = 0.2 \text{ keV}$  or  $T = 2.3 \times 10^6 \text{ K}$  as assumed in the analysis of WHIM spectra, which was also suggested to be reasonable

<sup>4</sup> <http://www.atomdb.org>

<sup>5</sup> The oxygen abundance is assumed to be  $\text{O}/\text{H} = 8.51 \times 10^{-4}$ .

based on the two component fit to the  $r = 8' - 12'$  spectra (§3.1). Then substituting  $C(2.3 \times 10^6 \text{ K})$ ,  $Z = 0.2$  solar, our measurement of the O VIII surface brightness under the Gaussian model yields

$$\delta = 319 \pm 62 (< 443) \left( \frac{Z}{0.2 Z_{\odot}} \right)^{-1/2} \left( \frac{L}{2.5 \text{ Mpc}} \right)^{-1/2}, \quad (3)$$

$$\delta = 283 \pm 81 (< 446) \left( \frac{Z}{0.2 Z_{\odot}} \right)^{-1/2} \left( \frac{L}{2.5 \text{ Mpc}} \right)^{-1/2}, \quad (4)$$

for  $r = 8' - 12'$  and  $12' - 16'$ , respectively. In the above calculation, the  $1\sigma$  error including both statistical and systematic uncertainties is quoted and the value in the parenthesis indicates the  $2\sigma$  upper limit. Note that  $L = 2.5 \text{ Mpc}$  was assumed because the spectral integration area of each filament region is approximated by a square, 2.5 Mpc on a side.

Similar values can be obtained if the limits on the O VII line and the APEC normalization are substituted, suggesting that the measurement is less affected by the choice of the spectral model. The results are summarized in Table 4. In §5.1, we considered the impact of possible contamination from the O I line on the WHIM measurement. The spectral fitting by ii) the Gaussian model plus the O I line gave a limit comparable to Equations 3–4, i.e.,  $\delta = 150 (< 479)$  and  $189 (< 513)$  respectively for  $r = 8' - 12'$  and  $12' - 16'$ .

The present result is comparable to that estimated near the virial radius of A2744 (Eckert et al. 2015) and those in other clusters (Takei et al. 2007; Kaastra et al. 2003); and also agrees with the theoretical prediction by Cen & Ostriker (2006), which suggested that the baryon overdensity ranges from 1 to 300, within the measurement errors.

## 5.2 Future prospects of the WHIM search

Our Suzaku observations suggest that X-ray spectroscopy of filaments around galaxy clusters will provide an important clue in the search for the densest part of the WHIM. By utilizing future non-dispersive, high-resolution X-ray spectrometer onboard DIOS (Ohashi et al. 2014) and Athena (Barcons et al. 2015), emission lines from ionized ions of intergalactic warm-hot gas are expected to be more clearly detected. The X-IFU micro-calorimeter onboard Athena will achieve a superior energy resolution of approximately 2.5 eV (Ravera et al. 2014; Gottardi et al. 2016).

To examine the detectability of the WHIM, we simulate the X-IFU spectra of the A2744 filament using `simx` version 2.4.1<sup>6</sup>. The APEC model with  $kT = 0.2 \text{ keV}$ ,  $Z = 0.2$  solar,  $z = 0.3$ , and  $\delta = 100, 200$ , and 400 were assumed. An example of the X-IFU

simulation is shown in Figure 6. In the case of  $\delta = 100$ , the count rates of O VII and O VIII lines are 175 and 210 (counts/100ks), respectively. Thus if  $\delta > 100$ , we expect to detect them with an exposure time of  $< 10 \text{ ks}$ . Since the centroid energy of the redshifted O VIII line overlaps with that of the Galactic O VII line, observing O VII and other lines to identify the WHIM is important. If the overdensity is high, we can detect not only the oxygen lines but also Fe and Ne lines. It should be possible to determine the redshift of the WHIM to an accuracy of about 0.1%.

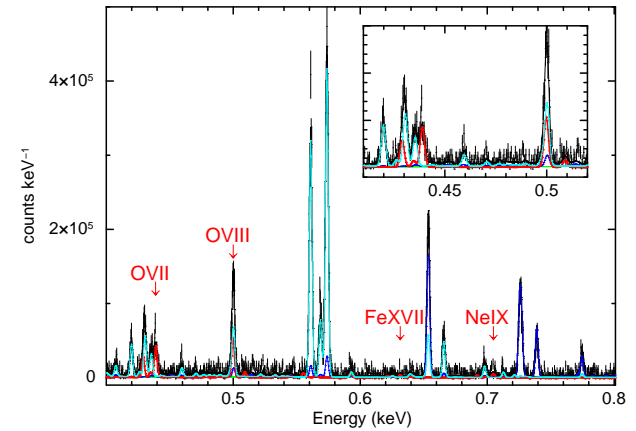


**Fig. 6.** Simulated Athena X-IFU spectrum of the WHIM in the case of  $\delta = 200$  and an exposure time of 20 ks (black cross). The spectral components are indicated by different colors: WHIM (red), CXB (green), LHB (cyan), and MWH (blue). Blow-up of the X-IFU spectrum in the 0.41–0.52 keV band is also shown.

## 5.3 ICM shock structure at the radio relic

In §4, we confirmed the presence of a temperature drop across the radio relic, which suggests that the cluster has experienced shock heating due to a merger. From the Rankine-Hugoniot shock condition with the ratio of specific heats  $\gamma = 5/3$ , the ratio of pre-shock ( $T_1$ ) and post-shock ( $T_2$ ) temperatures is related to the Mach number  $M_X$  through the following relationship (Landau & Lifshitz 1959):

$$\frac{T_2}{T_1} = \frac{5M_X^4 + 14M_X^2 - 3}{16M_X^2}. \quad (5)$$

From the observed ICM temperatures,  $T_1 = 1.7 \pm 0.2 \text{ keV}$  ( $8' < r < 12'$ ) and  $T_2 = 9.0 \pm 1.5 \text{ keV}$  ( $5' < r < 8'$ ), we obtain  $M_X = 3.7 \pm 0.4$ .

From the XMM-Newton observation, an X-ray surface brightness jump was found at the location of the radio relic (Eckert et al. 2016), indicating a weak shock with the Mach number of  $1.7^{+0.5}_{-0.3}$ . In addition, the spectral index of synchrotron emission from the radio relic (Orrú et al. 2007) yields a Mach number of  $M_{\text{radio}} = 1.7 - 2.5$ . The Mach number evaluated from our X-ray analysis is marginally higher than the above two measurements, however, we consider that it provides an-

<sup>6</sup> RMF (athena\_xifu\_rmf\_v20150327.rmf), ARF (athena\_xifu\_1190\_onaxis\_pitch265um\_v20150327.arf) response files and the instrumental background file (int1arcmin2\_athena\_xifu\_1190\_onaxis\_pitch265um\_v20150327.pha) were used.



other piece of evidence that the gas was shock heated via mass accretion along the filament.

## Acknowledgments

We are grateful to the Suzaku team members for satellite operation and instrumental calibration. We also thank the anonymous referee and Koji Mori for useful comments. This work was supported in part by JSPS KAKENHI grant 16K05295, 25247028 (NO). Y.Y.Z. acknowledges support by the German BMWi through the Verbundforschung under grant 50 OR 1506. H.A. is supported by a Grant-in-Aid for JSPS Fellows (26-606). H.A. acknowledges the support of NWO via a Veni grant. This research made use of data obtained from Data ARchives and Transmission System (DARTS), provided by Center for Science-satellite Operation and Data Archive (C-SODA) at ISAS/JAXA, and the NASA/IPAC Extragalactic Database (NED) which is operated by the Jet Propulsion Laboratory, California Institute of Technology, under contract with the National Aeronautics and Space Administration.

Dedicated to the memory of Dr. Yu-Ying Zhang, who made a great contribution to this field but sadly passed away at a young age.

## References

- Anders, E., & Grevesse, N. 1989, *Geochim. Cosmochim. Acta*, 53, 197
- Arnaud, M., Pointecouteau, E., & Pratt, G. W. 2005, *A&A*, 441, 893
- Barcons, X., Nandra, K., Barret, D., et al. 2015, *Journal of Physics Conference Series*, 610, 012008
- Bregman, J. N. 2007, *ARA&A*, 45, 221
- Boschin, W., Girardi, M., Spolaor, M., & Barrena, R. 2006, *A&A*, 449, 461
- Böhringer, H., Schuecker, P., Guzzo, L., et al. 2004, *A&A*, 425, 367
- Braglia, F., Pierini, D., Böhringer, H. 2007, *A&A*, 470, 425
- Cen, R., & Ostriker, J. P. 1999, *ApJ*, 514, 1
- Cen, R., & Ostriker, J. P. 2006, *ApJ*, 650, 560
- Davé, R., Cen, R., Ostriker, J. P., et al. 2001, *ApJ*, 552, 473
- Eckert, D., Jauzac, M., Shan, H., et al. 2015, *Nature*, 528, 105
- Eckert, D., Jauzac, M., Vazza, F., et al. 2016, *MNRAS*, 461, 1302
- Fujimoto, R., Mitsuda, K., Mccammon, D., et al. 2007, *PASJ*, 59, 133
- Fukugita, M., Hogan, C. J., & Peebles, P. J. E. 1998, *ApJ*, 503, 518
- Gottardi, L., Akamatsu, H., Bruijn, M. P., et al. 2016, arXiv:1604.00670
- Ibaraki, Y., Ota, N., Akamatsu, H., Zhang, Y.-Y., & Finoguenov, A. 2014, *A&A*, 562, A11
- Jauzac, M., Richard, J., Jullo, E., et al. 2015, *MNRAS*, 452, 1437
- Kaastra, J. S. 2004, *Journal of Korean Astronomical Society*, 37, 375
- Kaastra, J. S., Lieu, R., Tamura, T., Paerels, F. B. S., & den Herder, J. W. 2003, *A&A*, 397, 445
- Kalberla, P. M. W., Burton, W. B., Hartmann, D., et al. 2005, *A&A*, 440, 775
- Koyama, K., Tsunemi, H., Dotani, T., et al. 2007, *PASJ*, 59, 23
- Landau, L. D., & Lifshitz, E. M. 1959, *Course of theoretical physics*, Oxford: Pergamon Press, 1959,
- Lau, E. T., Nagai, D., Avestruz, C., Nelson, K., & Vikhlinin, A. 2015, *ApJ*, 806, 68
- Mitsuda, K., Bautz, M., Inoue, H., et al. 2007, *PASJ*, 59, 1
- Mitsuishi, I., Gupta, A., Yamasaki, N. Y., et al. 2012, *PASJ*, 64,
- Ohashi, T., Ishisaki, Y., Ezoe, Y., et al. 2014, *Proc. SPIE*, 9144, 91442Q
- Orrú, E., Murgia, M., Feretti, L., et al. 2007, *A&A*, 467, 943
- Ota, N., & Mitsuda, K. 2004, *A&A*, 428, 757
- Ota, N., Fujino, Y., Ibaraki, Y., Böhringer, H., & Chon, G. 2013, *A&A*, 556, A21
- Owers, M. S., Randall, S. W., Nulsen, P. E. J., et al. 2011, *ApJ*, 728, 27
- Ravera, L., Barret, D., den Herder, J. W., et al. 2014, *Proc. SPIE*, 9144, 91442L
- Reiprich, T. H., Basu, K., Ettori, S., et al. 2013, *Space Sci. Rev.*, 177, 195
- Sekiya, N., Yamasaki, N. Y., Mitsuda, K., & Takei, Y. 2014, *PASJ*, 66, L3
- Shull, J. M., Smith, B. D., & Danforth, C. W. 2012, *ApJ*, 759, 23
- Smith, R. K., Brickhouse, N. S., Liedahl, D. A., & Raymond, J. C. 2001, *ApJL*, 556, L91
- Takei, Y., Ohashi, T., Henry, J. P., et al. 2007, *PASJ*, 59, 339
- Wang, X., Hoag, A., Huang, K.-H., et al. 2015, *ApJ*, 811, 29
- Werner, N., Finoguenov, A., Kaastra, J. S., et al. 2008, *A&A*, 482, L29
- Yoshitake, H., Sakai, K., Mitsuda, K., et al. 2013, *PASJ*, 65,